Three-beam atom interferometer

H. Hinderthür, A. Pautz, V. Rieger, F. Ruschewitz, J. L. Peng, K. Sengstock, and W. Ertmer
Institut für Quantenoptik, Universität Hannover, Welfengarten 1, D-30167 Hannover, Germany
(Received 28 March 1997)

We present an atom interferometer based on the interference of three partial matter waves in three different internal and external states. Coherent laser excitation acts as a beamsplitter to create a superposition state of the ground state and two Zeeman sublevels of the metastable state of magnesium atoms. The interference pattern of the output ports shows high contrast and the characteristics of three-beam interferences as known from optical interferometry. In comparison to two-beam interferometry a reduction of the fringe width of $(32\pm8)\%$ is observed. This offers various possibilities for improved measurements of quantum-mechanical phases due to the internal atomic-state sensitive coupling of external potentials. This is demonstrated for the interaction of magnesium atoms with an external magnetic field. [S1050-2947(97)10509-1]

PACS number(s): 03.75.Dg, 07.60.Ly, 42.50.Vk, 32.80.Lg

I. INTRODUCTION

The extensive progress in the development of atom interferometry in recent years allowed the realization of an enormous variety of interferometric experiments, e.g., the observation of rotational and gravitational effects on atomic matter waves, the improved determination of atomic and molecular constants, and the investigation of topological phases and fundamental tests of quantum mechanics [1]. Various types of interferometers with different properties have been realized. They use either mechanical beam splitters (microfabricated gratings) [2–4] or beam splitters based on the exchange of photon momenta with light waves [5–9]. All of these interferometer concepts have the common principle of coherently recombining two partial waves with a definite phase relation. Interference of more than two partial waves is a new subject in atom optics.

As well known from photon optics, multiple-beam interferometers offer an increased sensitivity on the relative phase between the interfering partial waves. Therefore, multiple-beam atom interferometers will allow a new generation of precision measurements. A first atom interferometer with multiple beams where the signal at the output ports consists of a mixture of two-, three-, four-, and five-beam interferences has been realized recently [10]. The scheme discussed here consists of a pure three-beam interferometer with considerably high contrast. The setup allows direct switching from two-beam interference to three-beam interference in order to demonstrate the improvement in sensitivity of the three-beam interferometer. Due to the different internal states occupied by the three partial waves within the interferometer, highly sensitive measurements of electromagnetic potentials that couple to the electronic wave function are possible.

The paper is organized as follows: in Sec. II a purely mechanical interpretation of the interferometer concept is given. Section III contains a detailed quantum mechanical calculation of the expected interferometer signals. The experimental results of a three-beam magnesium (Mg) atom interferometer are discussed in Sec. IV.

II. CONCEPT

Our interferometer is based on the coherent splitting of atomic de Broglie waves by light fields resonant with an optical transition to a metastable internal state. The basic concept is an extension of the Ramsey-Bordé atom interferometer that consists of four traveling laser waves resonant with a two-level atomic system [11]. The interaction with four laser fields splits and subsequently recombines the atomic wavefunction by the exchange of photon energy and photon momentum between the laser fields and the atom. The phase shift between the two interfering partial waves is due to momentum transfer that is perpendicular to the direction of the laser beams as discussed in [7]. We follow this approach to present the basics of our interferometer concept.

Figure 1(c) shows a part of the recoil diagram of the interferometer. Paths that do not contribute to the three-beam interference are excluded. In the first interaction region a coherent superposition of three internal states is prepared. These three partial waves transversely and longitudinally split within the interferometer due to the absorbtion and emission of photons with different k-vectors. Whereas for the original Ramsey-Bordé interferometer the internal structure of the atom is regarded as a two-level system, we consider a three-level v system, e.g., the $J=0\text{-}J'=1$ intercombination transition in alkaline earth elements [Fig. 1(a)]. A weak magnetic field that is superimposed on the interferometer splits the Zeeman sublevels of the upper state by an energy $\Delta E=\hbar\Omega_B$, where Ω_B is the Larmor precession frequency. This magnetic splitting has to be small compared to the interaction broadening given by the traveling time τ of the atoms through the laser wave regions ($\Omega_B<1/\tau$). The four laser waves are linearly polarized perpendicular to the magnetic field that defines the quantization axis.

In this configuration the first laser beam prepares a superposition state of the ground state and the two Zeeman sublevels $m=-1$ and $m=+1$. Energy and momentum conservation for the absorbtion of a single photon with frequency ω_L demand

$$\frac{\vec{p}_0^{\,2}}{2M}+\hbar\omega_L=\frac{(\vec{p}_0+\hbar\vec{k})^2}{2M}+\hbar\omega_0+m\hbar\Omega_B, \qquad (1)$$

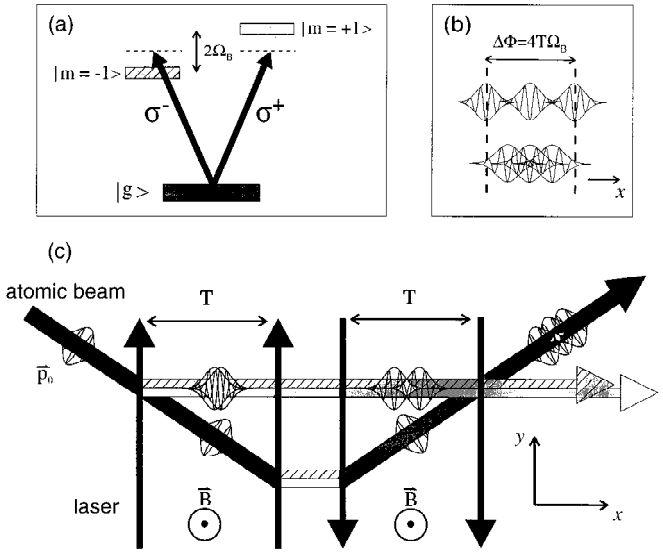

FIG. 1. (a) Level scheme of the $J=0\rightarrow J'=1$ transition in ^{24}Mg. (b) Magnetic-field-dependent separation between the interfering wave packets at the interferometer exit for two different magnetic-field strengths. The spatial separation is caused by the absorbtion of different k vectors from the laser beams. (c) Relevant part of the recoil diagram of the three-beam atom interferometer. Three wave packets with different internal and external degrees of freedom separate while passing through the interferometer. The interference signal is the number of atoms in the ground state at the exit as a function of the magnetic-field strength.

where ω_0 denotes the resonance frequency for the intercombination transition for magnetically unshifted excited states, $\vec{k}$ is the wave vector of the absorbed photon, $\vec{p}_0$ is the momentum of the incident ground-state atom, and M is the atomic mass. Introducing the laser detuning $\Delta=\omega_L-\omega_0$ and the photon recoil shift $\delta=\hbar k^2/2M$, Eq. (1) can be simplified to

$$\vec{k}\cdot(\vec{p}_0+\hbar\vec{k})/M=\Delta+\delta-m\Omega_B\,. \tag{2}$$

Thus, for $(\Delta+\delta)\neq m\Omega_B$ the atom absorbs a photon with a nonvanishing longitudinal momentum component k_x. While the transverse momentum transfer in the y direction is compensated in the following laser zones this longitudinal momentum difference between the partial waves leads to a spatial displacement of the atomic partial waves at the interferometer exit. The absorbtion of slightly different k vectors requires a k-vector spectrum in the interaction region as present in all focused light beams due to the x-p-uncertainty relation. The spatial displacement of the excited-state waves in the upper path relative to the ground-state wave in the lower path corresponds to a phase difference

$$\Delta\Phi=2T(\Delta+\delta-m\Omega_B). \tag{3}$$

Here $T=D/v_x$ denotes the time of flight between first and second or third and fourth laser zone, respectively. Therefore the relative phase difference between the two wave packets in the $m=-1$ and $m=+1$ excited states traveling along the upper path in Fig. 1 is $\Delta\Phi=4T\Omega_B$ when the wave packets exit the interferometer. Equation (3) indicates that there are two independent parameters, laser frequency and magnetic field, which can be used to change the relative phases and therefore scan the interference pattern. The wave packet traveling along the lower path in Fig. 1(c) can be regarded as a reference wave because its evolution in space is in good approximation independent of laser frequency and magnetic-field strength.

Multiple-beam interference in photon optics is characterized by a constant relative phase shift between all interfering partial waves [12]. In the three-beam atom interferometer this condition is fulfilled by locking the laser frequency on resonance $(\Delta+\delta=0)$ and scanning the magnetic-field strength [Fig. 1(b)]. Hence, we expect typical multiple-beam interference signals analogous to those for the diffraction at a triple slit in photon optics. For laser-frequency scans the relative phases between the three partial waves are different resulting in an asymmetrical interference pattern.

III. DETAILED CALCULATION

In what follows, we will calculate the interference signal at the two exit ports of the interferometer as a function of laser frequency and magnetic-field strength. We use the concept of momentum families as described in detail in [13]. First the complete interaction matrices for the laser atom interaction regions and the matrices for the free evolution regions are calculated. The interference signal is given by the product of the individual transition amplitudes of subsequent interactions with all four laser beams and the magnetic field.

The interaction between the four laser beams and an atom with an initial momentum of $\vec{p}_0$ leads to the population of momentum states which differ from $\vec{p}_0$ by a multiple of the photon momentum $\hbar\vec{k}$. It is assumed that the Rabi frequency in each individual interaction region leads roughly to a $\pi/2$ excitation. Thus, multiple photon exchange can be neglected. Additionally, we assume a lifetime of the excited state which is long compared to the time of flight of the atoms through the interferometer. Therefore, neglecting spontaneous emission, it is sufficient to take into account only one closed momentum family

$$F_n=\{|m=+1,\vec{p}_0+(n\pm1)\hbar\vec{k}\rangle,|m=-1,\vec{p}_0+(n\pm1)\hbar\vec{k}\rangle,|g,\vec{p}_0+n\hbar\vec{k}\rangle\},$$

where g is the notation for the ground state, and n is the net number of photon momentum quanta exchanged with the field. The plus or minus sign stands for positive or negative y direction of the appropriate laser beam. This momentum family is the basis for our following calculation in matrix representation.

A. Laser-atom interaction

The Schrödinger equation in the rotating-wave approximation is governed by the Hamiltonian

$$H_{L-A}=\frac{\hbar}{2}\begin{pmatrix}\lambda_e-\Delta+\Omega_B & 0 & \sqrt{\frac{1}{2}}\Omega_0\\ 0 & \lambda_e-\Delta-\Omega_B & \sqrt{\frac{1}{2}}\Omega_0\\ \sqrt{\frac{1}{2}}\Omega_0 & \sqrt{\frac{1}{2}}\Omega_0 & \lambda_g\end{pmatrix}_{F_n}, \tag{4a}$$

where λ_g and λ_e are the eigenvalues of the momentum operator $\hat{p}^2$ for ground- and excited-state that represent the contributions of the kinetic energy,

$$\lambda_g=\left\langle g,\vec{p}_0+n\hbar\vec{k}\left|\frac{\hat{p}^2}{\hbar M}\right|g,\vec{p}_0+n\hbar\vec{k}\right\rangle=\frac{p_0^2}{\hbar M}+2n\frac{\vec{p}_0\cdot\vec{k}}{M}+n^2\delta, \tag{4b}$$

$$\lambda_e=\left\langle m=\pm1,\vec{p}_0+(n\pm1)\hbar\vec{k}\left|\frac{\hat{p}^2}{\hbar M}\right.\right.\times\left|\langle m=\pm1,\vec{p}_0+(n\pm1)\hbar\vec{k}|\rangle\right.=\frac{p_0^2}{\hbar M}+2(n\pm1)\frac{\vec{p}_0\cdot\vec{k}}{M}+(n\pm1)^2\delta.$$

Both of the upper states couple to the ground state via the Rabi frequency Ω_0. Equation (4) can be further simplified if we make a transformation into the basis of the laser polarization $F_n'=\{|\mathfrak{nc},\vec{p}_0+(n\pm1)\hbar\vec{k}\rangle,|\mathfrak{c},\vec{p}_0+(n\pm1)\hbar\vec{k}\rangle,|g,\vec{p}_0+n\hbar\vec{k}\rangle\}$, where the internal states $|\mathfrak{c}\rangle=1/\sqrt{2}(|m=+1\rangle-|m=-1\rangle)$ and $|\mathfrak{nc}\rangle=1/\sqrt{2}(|m=+1\rangle+|m=-1\rangle)$ are linear combinations of the energy eigenstates. $|\mathfrak{nc}\rangle$ does not couple to the light field. The Hamiltonian in the rotated basis F_n' reads

$$H_{L-A}=\frac{\hbar}{2}\begin{pmatrix}\lambda_e-\Delta & \Omega_B & 0\\ \Omega_B & \lambda_e-\Delta & \Omega_0\\ 0 & \Omega_0 & \lambda_g\end{pmatrix}_{F_n'}. \tag{5}$$

Assuming $\Omega_B\ll\Omega_0$, which means that the Larmor precession of the atomic magnetic dipole vector is slow compared to the rate of population transfer by the laser excitation, we neglect Ω_B in the off-diagonal elements within the laser interaction zones. This condition is clearly fulfilled under typical experimental conditions. We obtain the time propagator of the atomic state as the solution of the Schrödinger equation

$$U_{L-A}(\tau)=\exp\left(-\frac{i}{\hbar}H_{L-A}\tau\right), \tag{6}$$

where τ is the interaction time between laser and atom.

B. Free evolution between the laser zones

Between the laser zones the time evolution is governed by the Hamiltonians of the unperturbed internal energy H_0 and the magnetic field H_B. Since H_0 and H_B commute, the two contributions can be separated,

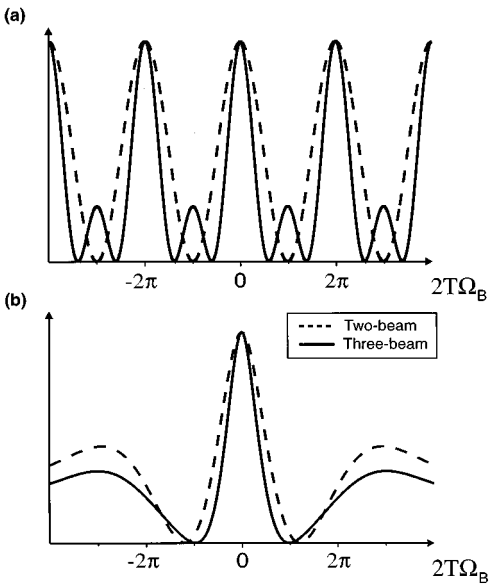

FIG. 2. Calculated interference signals for the three-beam interferometer (solid lines). The pulse area of the excitation pulse is optimized for best signal contrast ($\Omega_0\tau=0.61\pi$). The dashed lines are calculated two-beam signals (optimized pulse area in this case: $\Omega_0\tau=\frac{1}{2}\pi$). (a) Signals for a monochromatic atomic beam. (b) Signals for a thermal atomic beam.

$$U_{FE}(T)=\exp\left(-\frac{i}{\hbar}(H_0+H_B)T\right)=U_0(T)U_B(T), \tag{7a}$$

with

$$U_0=\begin{pmatrix}e^{-i(\Delta-\lambda_e)T} & 0 & 0\\ 0 & e^{-i(\Delta-\lambda_e)T} & 0\\ 0 & 0 & e^{-i\lambda_gT}\end{pmatrix}_{F_n'} \tag{7b}$$

and

$$U_B=\begin{pmatrix}\cos(\Omega_BT) & -i\sin(\Omega_BT) & 0\\ -i\sin(\Omega_BT) & \cos(\Omega_BT) & 0\\ 0 & 0 & 1\end{pmatrix}_{F_n'}. \tag{7c}$$

Equation 7(c) displays the coherence between the two excited states $|\mathfrak{c}\rangle$ and $|\mathfrak{nc}\rangle$. Note that this coherence is the well-known Hanle effect that describes the precession of a light-induced magnetic-dipole moment under the influence of a homogeneous magnetic field [14]. While the laser coupling between $|g\rangle$ and $|\mathfrak{c}\rangle$ is restricted to the laser zones the Hanle coupling between $|\mathfrak{c}\rangle$ and $|\mathfrak{nc}\rangle$ is taking place throughout the whole interferometer length.

The probability for finding an atom in the ground-state exit of the three-beam interferometer is finally given by

$$P_g=|\langle g,\vec{p}_0|U_{L-A}(\tau)U_B(T)U_0(T)U_{L-A}(\tau)\times U_{L-A}(\tau)U_B(T)U_0(T)U_{L-A}(\tau)|g,\vec{p}_0\rangle|^2. \tag{8}$$

Here the short traveling time between the second and third interaction region can be neglected. Figure 2(a) shows sig-

nals calculated from the expressions derived above assuming a monochromatic atomic beam. The signal shape depends on the laser intensity that defines the beam splitter ratio. The laser parameters are optimized to get $\frac{2}{3}$ of the population in the excited states after the first interaction zone (0.61π pulse). This yields a symmetric beam splitter ratio of $\frac{1}{3}$ for each of the three beams. For comparison, two-beam Ramsey fringes are plotted additionally, showing a purely sinusoidal behavior. The resulting interference signal displays all the characteristics of multiple-beam interferometry well known from photon optics, especially the main maxima become sharper by 41% and additional secondary maxima at phase differences of odd multiples of π appear.

Figure 2(b) displays calculated signals where the Maxwell-Boltzmann velocity distribution for a thermal atomic beam is taken into account. This situation can be compared to white light interference in photon optics. As a consequence of the limited coherence lengths the overlap of all three wave packets decreases with increasing phase shift and the overlap between each of the outer wave packets and the central reference wave gives a significant contribution to the signal. This is indicated in Fig. 1(b). Thus, the three-beam interference contributes mainly for $\Delta\Phi=0$. For larger phase shifts the signal is dominated by interferences between two waves. For that reason the secondary maxima in the signal disappear. But the width of the central fringe which corresponds to pure interferences between three waves is still reduced by 32% compared to that of the pure two-beam interference signal.

IV. EXPERIMENTAL SETUP AND RESULTS

The experimental setup is based on a four zone optical Ramsey-Bordé interferometer. A thermal Magnesium beam crosses two pairs of traveling light fields derived from a high-resolution dye-laser spectrometer at 457 nm. The four light zones are realized by reflecting a single laser beam using retroreflectors each consisting of a lens and a mirror at the focus of the lens. The experimental setup is depicted in Fig. 3. Details of the apparatus are described elsewhere [15]. The Zeeman shift of the $^3P_1$ sublevels is $\Omega_B=m\gamma B$ ($\gamma=2\pi\times2.1\times10^4$ MHz/T) and the average velocity in our thermal beam is about $\bar{v}=700$ m/s. The distances between the first and second respectively third and fourth laser beam are 4.5×10^{-3} m. The laser waists are about 5×10^{-4} m. Thus, a magnetic-field strength of a few microtesla leads to a phase shift of $\Delta\Phi=4\pi$ at the interferometer exit. Therefore,

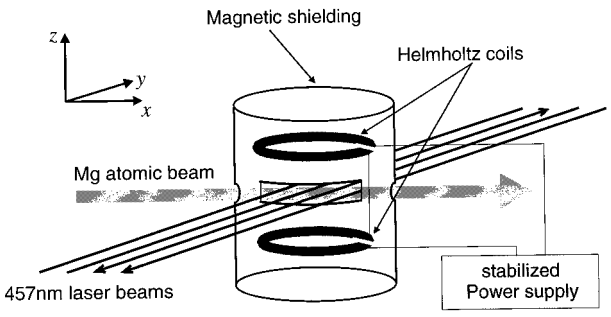

FIG. 3. Part of the experimental setup. Details are given in the text.

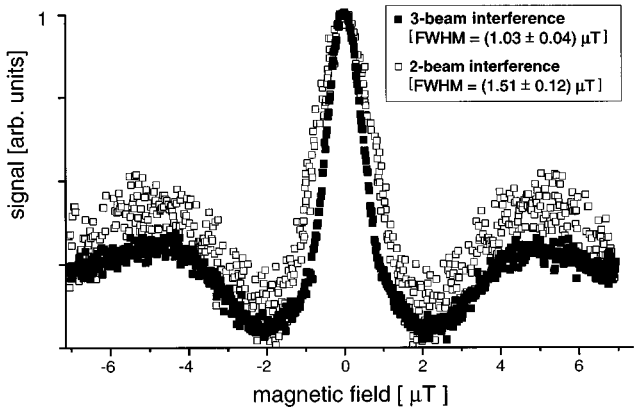

FIG. 4. Experimental data for three-beam (solid dots) and two-beam (open dots) interferences as a function of the magnetic-field strength. Contributions of the incoherent background are subtracted. For the three-beam interference a clear narrowing of the interference pattern can be observed.

careful magnetic shielding of the interferometric region is essential to preserve interference. Homogeneous compensation fields in addition to a specially designed μ metal can inside the vacuum chamber reduce the magnetic field of the earth and stray fields. Inside the can a pair of Helmholtz coils made of two copper rings (diameter 55 mm), which are driven by a stabilized current supply produce a magnetic field perpendicular to the interferometer plane. We estimate the residual inhomogeneties of the fields to be less than 10 nT.

Figure 4 shows experimental data for the realization of an atomic three-beam interferometer. The number of atoms in the ground-state exit of the interferometer is plotted as a function of the magnetic-field strength. To obtain higher detection efficiency we do not measure the ground-state population directly, but detect the fluorescence from atoms in the two excited states which is, due to particle conservation, exactly complementary to the ground-state exit signal (i.e., the data in Fig. 4 is equal to $1-$fluorescence signal). Contributions of the incoherent background are subtracted. Three-beam interference is achieved by scanning a weak magnetic field while the laser frequency is locked on resonance with the $^1S_0$-$^3P_1$ transition ($\Delta+\delta=0$). For comparison a pure two-beam interference where only two wave packets take part in the interference process is presented in addition. To realize this we introduced a large offset magnetic field $B=\gamma\Omega_{B\,\mathrm{off}}$ to strongly separate the two wave packets in the upper paths. An additional offset laser detuning Δ_{off} shifted the upper path wave packets and allowed an overlap in the reference wave and the wave packet in the $m=+1$ state of the upper path. Thus, as an effect of the limited atomic coherence lengths we have the possibility to directly compare two- and three-beam interference. The offset magnetic field for the two beam case is subtracted in the magnetic-field axis of Fig. 4. To allow direct comparison both traces are normalized to 1.

The shape of the experimental signals is in good agreement with the calculated data for a thermal atomic beam [Fig. 2(b)]. As an effect of the atomic velocity spread the secondary maxima of the three-beam interference vanish and the first-order main maxima of both signals are shifted to

higher magnetic fields corresponding to phases of more than 2π. The central fringes of the signals, which are only weakly affected by the atomic velocities, show the predicted narrowing for interference of three beams. The full width at half maximum values are $(1.03\pm0.04)\ \mu T$ for three beams and $(1.51\pm0.12)\ \mu T$ for two beams, e.g., the width of the main maximum is reduced by $(32\pm8)\%$ which is in excellent agreement with the theory. The lower signal-to-noise ratio for the two-beam interference is a direct consequence of the fact that the third wave packet in the $m=-1$ state does not take part in the interference but its amplitude still contributes to the background signal.

Figure 4 also demonstrates the increased sensitivity of such a multiple-beam interferometer for the precision measurement of weak magnetic fields. The absolute magnetic-field sensitivity we get in the present experiment is about $5.2nT/\sqrt{\min}$. This value is comparable to another interferometric experiment [16] and is directly limited by the short interaction times between atoms and magnetic field in our thermal beam interferometer. Using cold atom—interferometry [17], where the interfering atoms are captured in a magneto-optical trap and the beam splitters are realized by laser pulses, the interaction times can be easily increased by a factor of 100. In addition, this leads to an interesting possibility to build an atomic magnetometer with a ''point-like atomic ensemble as a sensor. Furthermore, an improvement of the signal-to-noise-ratio by a factor of 100 due to a more efficient detection scheme [17] should provide sensitivities below $1pT/\sqrt{\min}$.

The concept of three-beam interferences that has been described here can easily be extended to multiple-beam interferences using atoms with a multilevel structure in the ground and excited states. This allows, as in classical optics, a further increase of the interferometer sensitivity.

The demonstration of an alternate optical frequency standard is a strong motivation for atom interferometry experiments with magnesium atoms. In previous experiments the magnetic field uncertainty has been a significant limitation for the accuracy of the line center (influence of the magnetic-field uncertainty: $\delta\nu/\nu_0\approx1.5\times10^{-16}$) [15]. The further minimization of stray magnetic fields for our high-resolution spectroscopy experiments will be an additional future application for our interferometer concept.

V. CONCLUSION

We have presented a type of atom interferometer where three partial atomic de Broglie waves prepared by coherent excitation of different electronic states take part in the interference. The interference signals are of high contrast and in good agreement with the calculations. They show the typical characteristics of multiple-beam interference that are well known from photon optics. The three partial waves in our interferometer have different external and internal states. Therefore, our concept in principle opens the possibility for improved precision measurements of potentials which couple to the internal atomic state. We have demonstrated this in the case of a magnetic field where the sensitivity is clearly increased compared to the conventional two-beam interferometer. To increase the number of interfering beams it is possible to use atoms with a multilevel structure in the metastable state (for example) ^{25}Mg or molecules with its complex vibrational-rotational level structure. The reduction of stray magnetic fields for high-resolution spectrocopy is a future application for this new concept.

ACKNOWLEDGMENTS

This research was supported by the Deutsche Forschungsgemeinschaft. J.L.P. acknowledges support by the DAAD.

[1] For an overview see *Atom Interferometry*, edited by P. Berman (Academic, New York, 1997).
[2] O. Carnal and J. Mlynek, Phys. Rev. Lett. **66**, 2689 (1991).
[3] D. W. Keith, C. R. Ekstrom, Q. A. Turchette, and D. E. Pritchard, Phys. Rev. Lett. **66**, 2693 (1991).
[4] F. Shimizu, K. Shimizu, and H. Takuma, Phys. Rev. A **46**, 17 (1992).
[5] M. Kasevich and S. Chu, Phys. Rev. Lett. **67**, 181 (1991).
[6] F. Riehle, Th. Kisters, A. Witte, J. Helmcke, and C. J. Bordé, Phys. Rev. Lett. **67**, 177 (1991).
[7] U. Sterr, K. Sengstock, J. H. Müller, D. Bettermann, and W. Ertmer, Appl. Phys. B **54**, 341 (1992).
[8] E. M. Rasel, M. K. Oberthaler, H. Batelaan, J. Schmiedmayer, and A. Zeilinger, Phys. Rev. Lett. **75**, 2633 (1995).
[9] D. M. Giltner, R. W. Mc Gowan, and S. A. Lee, Phys. Rev. Lett. **75**, 2638 (1995).
[10] M. Weitz, T. Heupel, and T. W. Hänsch, Phys. Rev. Lett. **77**, 2356 (1996).
[11] C. J. Bordé, Phys. Lett. A **140**, 10 (1989).
[12] See, for example, E. Hecht and A. Zajac, *Optics* (Addison-Wesley, Reading, 1974).
[13] C. J. Bordé, C. Salomon, S. Avrillier, A. van Lerberghe, C. Bréant, D. Bassi, and G. Scoles, Phys. Rev. A **30**, 1836 (1984).
[14] W. Hanle, Z. Phys. **30**, 93 (1924); **35**, 346 (1926).
[15] K. Sengstock, U. Sterr, J. H. Müller, V. Rieger, D. Bettermann, and W. Ertmer, Appl. Phys. B **59**, 99 (1994).
[16] J. Schmiedmayer *et al.*, J. Phys. II **4**, 2029 (1994).
[17] K. Sengstock, U. Sterr, G. Hennig, D. Bettermann, J. H. Müller, and W. Ertmer, Opt. Commun. **103**, 73 (1993).